HHS Public Access

Author manuscript

Nanoscale. Author manuscript; available in PMC 2023 February 10.

Published in final edited form as:

Nanoscale. ; 14(6): 2411–2418. doi:10.1039/d1nr07497k.

High affinity protein surface binding through co-engineering of nanoparticles and proteins

Moumita Ray[a], **Giorgia Brancolini**[b], **David C. Luther**[a], **Ziwen Jiang**[a], **Roberto Cao-Milán**[a], **Alejandro M. Cuadros**[a], **Andrew Burden**[a], **Vincent Clark**[a], **Subinoy Rana**[a], **Rubul Mout**[a], **Ryan F. Landis**[a], **Stefano Corni**[b,c], **Vincent M. Rotello**[a]

[a]Department of Chemistry, University of Massachusetts, 710 North Pleasant Street, Amherst, MA 01003, USA

[b]Center S3, CNR Institute of Nanoscience, via Campi 213/A, 41125 Modena, Italy

[c]Department of Chemical Science, University of Padova, Via Francesco Marzolo 1, 35131 Padova, Italy

Abstract

Control over supramolecular recognition between proteins and nanoparticles (NPs) is of fundamental importance in therapeutic applications and sensor development. Most NP-protein binding approaches use ‘tags’ such as biotin or His-tags to provide high affinity; protein surface recognition provides a versatile alternative strategy. Generating high affinity NP-protein interactions is challenging however, due to dielectric screening at physiological ionic strengths. We report here the co-engineering of nanoparticles and protein to provide high affinity binding. In this strategy, ‘supercharged’ proteins provide enhanced interfacial electrostatic interactions with complementarily charged nanoparticles, generating high affinity complexes. Significantly, the co-engineered protein-nanoparticle assemblies feature high binding affinity even at physiologically relevant ionic strength conditions. Computational studies identify both hydrophobic and electrostatic interactions as drivers for these high affinity NP-protein complexes.

Graphical Abstract

Author contributions

M.R., G.B., S.C., and V.M.R. designed the experiments. M.R., G.B., D.C.L, and V.M.R.. wrote the manuscript. M.R., S.R., and R.M. developed methodology for bacterial protein expression. D.C.L., Z.J., A.M.C., and A.B. expressed and purified recombinant proteins. Z.J. and R.F.L. synthesized gold nanoparticles. D.C.L., R.C.-M., A.B., and V.C. performed size analysis by DLS. G.B. and S.C. performed computational studies and interpreted results. M.R., Z.J., and A.M.C. performed binding studies and interpreted data. S.C. and V.M.R. oversaw the project.

†Electronic Supplementary Information (ESI) available: [Protein sequences and additional Fig.s.]. See DOI: 10.1039/x0xx00000x

Conflicts of interest

There are no conflicts to declare.

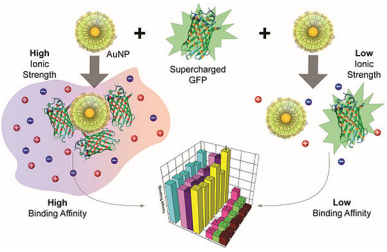

Supercharged proteins provide a strategy for high-affinity nanoparticle-protein binding at high ionic strength.

1. Introduction

Engineered nanoparticles (NPs) provide a powerful and flexible scaffold for interfacing with biologics.[1,2,3] Rational co-engineering of non-covalent interactions between NPs and proteins can aid in the creation of nanoparticle-protein supramolecular complexes with unique properties.[4,5] A range of supramolecular interactions[6–9] (ionic, hydrophobic, van der Waals, hydrogen, and coordination bonding) are involved and can be manipulated to generate these structures.[10,11,12] Finely tuneable nanoparticle size affords even further control over binding or functional attributes.[13,14,15] The resulting supramolecular complexes can act as robust bioconjugate systems and have been applied for a range of applications, from modulation of enzyme activity[16–19] and biological sensing,[20,21] to imaging[22,23,24] and therapeutic delivery.[25–30]

Generation of high-affinity discrete NP protein complexes for use at physiological conditions remains challenging.[31,32] Charged cationic gold NPs (AuNPs) can efficiently interact with negatively charged GFP (pI=5.9) in solutions of low ionic strength (pH 7.4) to form discrete nanoscale complexes. These complexes have been effectively utilized as molecular agents for the detection of metastatic mammalian cells as well as disease-relevant levels of biomarker proteins *in vitro*.[33,34] However while these complexes form readily under low ionic strength conditions, they were disrupted at physiologically relevant ionic strengths, limiting practicality in biological applications.[35]

In Nature, proteins with highly charged surface domains are often strongly associated with other proteins with complementary surface charge in the cellular cytoplasm and/or in cellular compartments.[36,37] Examples of these interactions include DNA duplexes,[38] leucine zippers,[39] and some specific protein-protein adducts such as cytochrome c (highly positive) and prothymosin-α (highly negative).[40,41] Complementary surface charges on the binding partners are responsible for high stability of these complexes under conditions of physiologically relevant ionic strength. We hypothesized that the highly charged interfaces observed in these biological systems could be employed to generate high affinity NP-protein interactions. We report here the use of this strategy to achieve remarkably high-affinity interactions between supercharged GFP[42,43] (high surface charge), and engineered AuNPs (Fig. 1). This interaction provides nanomolar NP-protein binding affinity even at physiologically relevant ionic strengths (100–200 mM), in strong contrast with that observed with wild-type GFP (*wt*GFP). Computational studies suggest that these strong interactions

arise from a synergistic combination of electrostatic and hydrophobic interactions enabled by the NP-protein interface. This new supramolecular motif provides a promising scaffold for the creation of new bioconjugate platforms for sensing, delivery, and other applications.

2. Results and Discussion

Multivalency is a key tool for achieving strong binding affinity.[44,45,46] Multivalent nanoparticle hosts were generated by functionalizing the monolayer of AuNPs (2 nm core diameter) with a cationic arginine-based ligand (Arg-NPs). We chose highly negatively charged GFP (−30GFP) as our model protein to interact with Arg-NPs. This −30GFP[42,43] is a variant of GFP in which 15 surface-exposed residues were mutated to negatively charged amino acids (Asp/Glu) (protein sequences are available in Supporting Information). We hypothesized that the Arg-NP would interact strongly with −30GFP through electrostatic and hydrogen bonding interactions.[47]

We first carried out dynamic light scattering (DLS) characterization to validate discrete NP-protein assembly formation. DLS analyses of particles alone demonstrated a slight reduction in hydrodynamic radius for Arg-NPs in solutions near physiological ionic strength (100 mM NaCl, Fig. S1). To further support these data, we performed a series of 100 ns molecular dynamics (MD) simulations of a single nanoparticle in aqueous environment with counterions at increasing ionic strengths. We observed that increasing solution ionic strength (from 0 mM) led to a reduction in the overall radius of the monolayer for both nanoparticles (Fig. S2). This is suggestive of monolayer compaction and is consistent with observations detailed in our previous reports.[48] Discrete assemblies with diameters ranging 50–70 nm were observed by DLS for −30GFP: Arg-NP mixtures (Fig. S3). Increasing Arg-NP concentration above a 1:4 protein: NP molar ratio produced a mixture of discrete assemblies and free particles (Fig. S4), indicating that at this ratio all proteins were bound. Similar results were obtained for complexation in low salt phosphate buffer (5mM PB) as for physiologically relevant salt concentrations (200 mM NaCl)

NP-protein binding affinity as a function of ionic strength

Gold nanoparticles strongly quench nearby fluorophores through efficient energy transfer to the gold core.[49,50] This fluorescence quenching was used to quantify the binding affinities of the Arg-NPs host with the GFP guests.[51] We titrated −30GFP with Arg-NPs in 5 mM PB (pH 7.4) solutions at a wide range of ionic strengths (NaCl, 0, 50, 100, 150, and 200 mM). Fluorescence intensity of the protein was gradually quenched with increasing concentration of Arg-NPs (Fig. 2 and Fig. S5). The complex binding constants (K_b) and association stoichiometries (n) were obtained through nonlinear least-squares curve-fitting analysis.[52]

Binding affinity between −30GFP and Arg-NPs remained relatively high across all ionic strengths examined (Fig. 2 and Table S1). Affinity between Arg-NPs and −30GFP was enhanced ~4 fold with an increase in ionic strength from 0 to 50 mM NaCl. With a further increase in salt concentration, K_b decreased but remained at least 2-fold higher than was observed in 5 mM PB, up to 125 mM NaCl. This result contrasts with previous studies where electrostatic interactions between nanoparticles and proteins were fully disrupted at 10–50 mM salt concentrations.[35] At higher temperatures (above 28°C) interaction strength

decreased with increasing ionic strength, as would be expected from progressive charge screening, however relatively high affinity (K_b = 1.686 ± 0.005 ×10^9 M^{-1}) was still observed at 37°C under physiologically relevant ionic strength conditions (Table S1).

Generality of the NP-supercharged protein co-engineering strategy was demonstrated by utilizing a positively charged GFP mutant (+36GFP) and carboxylate-terminated AuNPs (COOH-NPs). The +36GFP was constructed by Liu *et al.* by mutating 29 residues of *wt*GFP into positively charged amino acid residues (Lys/Arg).[42] The interaction between +36GFP and COOH-NPs produced discrete assemblies as demonstrated by DLS (Fig. S3). Fluorescence titrations (Fig. 3, Table S2) showed that +36GFP and COOH-NPs interacted with nanomolar affinity at all ionic strengths and temperatures studied. Interestingly, at low/ambient temperatures (22–28°C), K_b values showed non-monotonic behaviour with increasing ionic strength, as was observed with −30GFP: Arg-NP complexes. Depicted in Fig. 3, an initial increase in the ionic strength (up to 100 mM NaCl) enhanced K_b by ~7 fold, while further increasing ionic strength reduced binding affinity. Complexes between +36GFP: COOH-NP exhibited a K_b ~5 fold lower than that of −30GFP: ArgNPs complexes. This interaction still proved much stronger than that of *wt*GFP (native GFP, −7GFP) and Arg-NPs (Fig. S6, Fig. S7).

Binding was also examined between COOH-NPs and an engineered GFP variant with less positive charge (+15GFP). These partners did form discrete complexes, but K_b values were in the range of ~10^7 M^{-1}, almost 100-fold lower than that of +36GFP: COOH-NPs (Table S3, Fig. S8). These results collectively suggest that stability of GFP: NP assemblies is strongly reliant on the charge density of each component of the complex.

Computational studies of the interactions between GFP and AuNPs

We next utilized computational methods to probe the origins of the high affinity interactions observed between NPs and supercharged proteins. A series of representative Brownian Dynamics (BD) simulations were performed under varied ionic strength with supercharged proteins and *wt*GFP.[53,54] These simulations modelled the interaction between a single AuNP and a single GFP protein, with the aim of better understanding the interfacial recognition between the two binding partners.[55,56]

We first focused on the binding of a single Arg-NP (represented as $Au_{144}[L_{60}]^{+60}$ [L=$S(CH_2)_9(OC_2H_4)_4$Arg]) to a single GFP protein variant, either *wt*GFP (−7GFP) or −30GFP. The initial structures of the single GFP proteins and Arg-NP were relaxed with 200 ns of fully atomistic molecular dynamics simulations with GROMACS2020.[57] Rigid-body docking (coded in SDA 7.2)[58,59] was applied to identify the possible adsorption orientations of protein on the Arg-NP surface and corresponding driving forces. Trajectories (5,000) were generated at each solution ionic strength (10, 50, 100, and 200 mM NaCl). Reduced charges were included in the docking to account for the number of Cl^- counterions found within Arg-NP monolayer after 200 ns of MD simulation at each ionic strength (Fig. S9). The reduced charges reflected the partially screened total charge of the Arg-NP monolayer due to counterions at different ionic strengths, which further affects the overall charge experienced by the GFP proteins during binding. The adsorption free energies

and trajectories of protein-AuNP complexes were clustered to identify different protein orientations.

Docking studies revealed different orientations of *wt*GFP: $Au_{144}[L_{60}]^{+60}$ and −30GFP: $Au_{144}[L_{60}]^{+60}$ complexes at different ionic strengths. For each ionic strength condition, the most populated complex as ranked by size was selected as shown in Fig. 4. The amino acid residues most frequently involved in interaction are displayed. Significantly, it was observed that recognition between these two binding partners could occur through several different specific interactions. This result supports previous findings that a single AuNP can bind as many as 3 protein partners to form a hierarchical superstructure.[48]

Motivated by these results we sought to examine the fundamental forces driving particle-protein interaction. The interaction between protein and AuNPs can be described by three terms: 1: electrostatic interaction energy (U_{EP}), dominated by contribution from charged amino acid side chains; 2: electrostatic desolvation energy of the protein: NP complex (U_{ds}^{e}) and 3: non-polar interactions (U_{ds}^{h}). As shown in Table 1, at 10 mM NaCl the total interaction energy (U_{Repr}) of −30GFP: Arg-NP was approximately two-fold higher than that of *wt*GFP: Arg-NP. With increasing ionic strength, total interaction energy of −30GFP: Arg-NP remained consistently ~1.5 fold higher than that of the *wt*GFP: Arg-NP interaction. At lower salt concentrations (10, 50 mM) binding was driven mainly by electrostatics (U_{EP}), with a smaller contribution from non-polar (hydrophobic) desolvation energy (U_{ds}^{h}), (Table 1, Fig. 4). With increased ionic strength (100 mM), electrostatic interaction slightly decreased, presumably due to charge screening by ions in solution. Interestingly, even under higher ionic strength conditions non-polar (hydrophobic) desolvation energy remained large and negative. The combination of the electrostatic interaction energy and non-polar (hydrophobic) desolvation energy kept the total interaction energy of −30GFP: Arg-NP high, ensuring stability of the protein: AuNP complex.

Related studies examined the docking of +36GFP with COOH-NPs (COOH-NPs were represented as $Au_{144}[L_{60}]^{-60}$ [$L=S(CH_2)_9(OC_2H_4)_4COO^-$]). As was observed in the −30GFP: ArgNP docking studies, total electrostatic interaction energy decreased with increasing salt concentration, but remained at least ~3-fold higher than *wt*GFP, even at 200 mM (Fig. S10 and Table S4). Interestingly, non-polar (hydrophobic) desolvation energy marginally increased with increasing ionic strength, slightly contributing to the interaction energy between the two components.

Docking results for *wt*GFP: Arg-NP binding predicted a total interaction energy ~2-fold lower than that of the −30GFP: Arg-NP interaction, with a substantial weakening at 200 mM. This significant reduction in the total interaction energy of *wt*GFP: Arg-NP interaction was reflected in the lower binding affinity of *wt*GFP: Arg-NP cluster at higher ionic strengths. These studies collectively demonstrate increased electrostatic affinity between AuNPs and complementarily charged GFP variants as compared to *wt*GFP, demonstrating their utility as a robust dual-component system.

3. Conclusions

In summary, we have demonstrated the ability of engineered proteins with high surface charge to form robust supramolecular assemblies with complementarily charged AuNPs. These discrete nanoscale particle-protein complexes were robust even at physiologically relevant ionic strength conditions that totally disrupt normal electrostatic NP-protein interactions. Computational docking studies further elucidated the electrostatic and hydrophobic forces responsible for interfacial recognition between binding partners. Taken together, these studies provide key insight into supramolecular binding and complexation between engineered proteins and complementarily charged nanoparticles. This strategy is highly generalizable and has potential for development of novel nanomaterials invaluable to biomedical and sensing applications.

4. Experimental

Cloning and over-expression of supercharged GFPs and *wt*GFP

Genetic engineering manipulation and protein expression were performed according to standard protocols. pET21d-GFP plasmid (Novagen)[60] containing 6x-His-tag at the N-terminus was used for *wt*GFP expression. −30GFP and +36GFP plasmids were gifts from Prof. David R. Liu, Harvard University, MA, US.[42,43] To remove 6x-His tag from +36GFP, thrombin cleavage site was added upstream of +36GFP sequence. Briefly, +36GFP was used as the template PCR with primers listed below. Subsequently, the PCR product was digested (using BamHI and HindIII restriction enzymes) and inserted into a pQE80 vector, downstream of nucleotides for 6X-histidine tag to construct pQE80–6x-His-Thombin-36GFP expression vector. Successful cloning was confirmed by DNA sequencing.

Forward primer:

5’- ACGATGGATCCCTTGTACCTCGAGGTTCTGGTGGCGCTAG −3’

Reverse primer:

5’- GTGTAAGCTTTTACTTGTAGCGTTCGTC −3’

To produce recombinant proteins, plasmids carrying −30GFP, +15GFP, +36GFP and *wt*GFP were transformed into *Escherichia coli* BL21 (DE3) strain. A transformed colony was picked up to grow small cultures in 50 mL 2XYT media at 37 °C for overnight. The following day, 10 mL of grown culture was inoculated into one-liter 2XYT media and allowed to grow at 37°C until OD reached 0.6. At this point, expression was induced by adding isopropyl-β-D-thiogalactopyranoside (IPTG, 1 mM final concentration) at 25°C. After 16 hours of incubation, the cells were harvested, and the pellets were lysed using 1% Triton-X-100/DNase-I in PBS containing 2M NaCl. Triton-X-100 treatment was performed for 30 min followed by DNase-I treatment for 15 min. Lysed cells were then centrifuged at 14,000 rpm for 30 min. The supernatant was collected. Proteins were purified from the supernatant using HisPur cobalt columns. The purity of native proteins was determined using 12% SDS-PAGE gel. For +15GFP and +36GFP protein, 6x-His tags were cleaved using thrombin agarose beads (Thrombin CleanCleave™ Kit, Sigma-Aldrich) as described in

the instruction manual. Next, +15GFP/+36GFP were passed through a HisPur cobalt column to remove the cleaved 6x-His tag. Further, the residual 6x-His tags were removed by a 10 kDa-MWCO (molecular weight cut off) filter.

Synthesis and characterization of nanoparticles

Carboxylate functionalized gold nanoparticles (COOH-NPs) and arginine functionalized gold nanoparticles (Arg-NPs) were synthesized according to a previous report.[61] Briefly, Brust-Schiffrin two-phase synthesis was used to synthesize pentane thiol-coated AuNPs with 2-nm core diameter.[62,63] The Murray place-exchange method was followed to obtain Arg-NPs or COOH-AuNP.[64] The monolayer protected nanoparticles were re-dispersed in water. Excess ligand/pentanethiol was removed by dialysis using a 10,000 MWCO snake-skin membrane. The final concentration was measured by UV spectroscopy at 502 nm. To assess particle quality, the nanoparticles were characterized by Zeta potential (surface charge) and dynamic light scattering (DLS, hydrodynamic diameter), as shown in Fig. S1.

Fluorescence titration

Fluorescence titration experiments between nanoparticles and proteins (supercharged GFPs and *wt*GFP) were carried out as previously described.[52] Briefly, the change of fluorescence intensity of supercharged GFPs and *wt*GFP at 510 nm was measured with an excitation wavelength of 475 nm at various concentrations of nanoparticles (0–320 nM) and ionic strength (0–200 mM) on a Molecular Devices SpectraMax M2 microplate reader (at 25–37°C). Quenching of fluorescence intensity arising from 50–100 nM GFP was observed with increased nanoparticle concentration. Nonlinear least–squares curve fitting analysis was carried out to estimate the binding constant (K_b) and association stoichiometry (n, [GFP]:[AuNP]) using a one site binding model. For salt dependent interactions (fluorescence titrations) between nanoparticles and supercharged GFPs and *wt*GFP, solutions were prepared by adding different amounts of NaCl in 5 mM phosphate buffer, pH 7.4. The titrations were carried out in triplicates and repeated at least twice with different batches of nanoparticles.

Modelling Studies

Rigid-body docking simulations were carried out using Brownian dynamics (BD) techniques with the ProMetCS continuum solvent model augmented with protein-AuNP interactions parameters.[65] The calculations were performed using the SDA version 7.2.2 software.[58,59] GFP structure was obtained by starting from NMR structure of the native state (PDB: 1GFL) and −30GFP and +36GFP were obtained by introducing the mutation along the sequence. Experimental salt concentrations (10 mM, 50 mM, 100 mM and 200 mM) were included as a non-specific screening effects on the electrostatic potential of the protein which was calculated using the APBS program.[66] For each ionic strength, reduced effective charges on Arg-NP were used to take into account the presence of 26 or 27 Cl^- ions within the Arg-NP monolayer (i.e. distances less than 2 nm from the Au core center) as resulted from 100 ns atomistic molecular dynamics. All titratable protein side chains were assigned by their standard protonation state at pH 6.8 with H++.[67] 5000 BD trajectories were computed, and the specified numbers of docked complexes were extracted directly from the runs and clustered with a clustering algorithm. The relative translational diffusion coefficient was

0.0135 Å^2/ps and the rotational diffusion coefficient for the protein was 3.92×10^{-5} in radian^2/ps. The simulation time step was set to 1.00 ps. Parameters for the calculation of hydrophobic desolvation energy/forces was set to −0.013 kcal/mole/Å^2 and that for the electrostatic desolvation energy/forces was set to 1.67.[68]

We remark that atomistic parameters for the Arg-NP and COO-NP were not available within the standard force fields and were developed within the GolP framework[69] including *ab initio* calculations for RESP charges.[70] Each NP was simulated for 200 ns at 300 K with explicit water and neutralizing counterions. For the 3D structures of the engineered supercharged and native protein sequences used in the experiments, homology modeling was performed. The homology models for the −30GFP, +36GFP and *wt*GFP were obtained by threading approach with the online software I-TASSER[71] and they were refined by 500 ns of standard MD at 300 K in explicit water and ions with GROMACS.[57] From the MD trajectories the clustering analysis was performed and representative structures for both proteins and AuNP were extracted and used in the rigid-docking.

Supplementary Material

Refer to Web version on PubMed Central for supplementary material.

Acknowledgements

Support from the NIH (EB022641 and DK121351, GM008515 to DCL) is acknowledged. −30GFP, +15GFP and +36GFP plasmids were gifts from Prof. David R. Liu, Harvard University, MA, USA.

References

1. Abdelsattar S, Dawoud A and Helal MA, Nanotoxicology, 2021, 15, 66–95. [PubMed: 33283572]
2. Luther DC, Huang R, Jeon T, Zhang X, Lee Y-W, Nagaraj H and Rotello VM, Adv. Drug Deliv. Rev, 2020, 156, 188–213. [PubMed: 32610061]
3. Geng Y, Amante JJ, Goel HL, Zhang X, Walker MR, Luther DC, Mercurio AM and Rotello VM, ACS Nano, 2020, 14, 15276–15285. [PubMed: 33164505]
4. Mosquera J, Zhao Y, Jang H-J, Xie N, Xu C, Kotov NA and Liz-Marzán LM, Adv. Funct. Mater, 2020, 30, 1902082.
5. Scaletti F, Hardie J, Lee Y-W, Luther DC, Ray M and Rotello VM, Chem. Soc. Rev, 2018, 47, 3421–3432. [PubMed: 29537040]
6. Tian X, Chong Y and Ge C, Front. Chem, 2020, 8, 446. [PubMed: 32587847]
7. Pinals RL, Chio L, Ledesma F and Landry MP, Analyst, 2020, 145, 5090–5112. [PubMed: 32608460]
8. Kopp M, Kollenda S and Epple M, Acc. Chem. Res, 2017, 50, 1383–1390. [PubMed: 28480714]
9. Yu Q, Zhao L, Guo C, Yan B and Su G, Front. Bioeng. Biotechnol, 2020, 8, 210. [PubMed: 32266237]
10. Chen and Ting AY, Curr. Opin. Biotechnol, 2005, 16, 35–40. [PubMed: 15722013]
11. Cooper WJ and Waters ML, Curr. Opin. Chem. Biol, 2005, 9, 627–631. [PubMed: 16257571]
12. Han G, Wang J-T, Ji X, Liu L and Zhao H, Bioconjug. Chem, 2017, 28, 636–641. [PubMed: 28035817]
13. Piella J, Bastús NG and Puntes V, Bioconjug. Chem, 2017, 28, 88–97. [PubMed: 27997136]
14. Kim, Han G, Toley BJ, Kim C-K, Rotello VM and Forbes NS, Nat. Nanotechnol, 2010, 5, 465–472. [PubMed: 20383126]

15. Jiang Y, Huo S, Mizuhara T, Das R, Lee Y-W, Hou S, Moyano DF, Duncan B, Liang X-J and Rotello VM, ACS Nano, 2015, 9, 9986–9993. [PubMed: 26435075]
16. You C-C, De M, Han G and Rotello VM, J. Am. Chem. Soc, 2005, 127, 12873–12881. [PubMed: 16159281]
17. You C-C, Agasti SS and Rotello VM, Chemistry, 2008, 14, 143–150. [PubMed: 17972262]
18. You C-C, Agasti SS, De M, Knapp MJ and Rotello VM, J. Am. Chem. Soc, 2006, 128, 14612–14618. [PubMed: 17090046]
19. Parveen R, Shamsi TN and Fatima S, Int. J. Biol. Macromol, 2017, 94, 386–395. [PubMed: 27746352]
20. Geng Y, Peveler WJ and Rotello VM, Angew. Chem. Int. Ed Engl, 2019, 58, 5190–5200. [PubMed: 30347522]
21. Geng Y, Chattopadhyay AN, Zhang X, Jiang M, Luther DC, Gopalakrishnan S and Rotello VM, Small, 2020, 16, e2002084. [PubMed: 32347000]
22. Kairdolf A, Qian X and Nie S, Anal. Chem, 2017, 89, 1015–1031. [PubMed: 28043119]
23. Kim S, Li X, Jiang Y, Yan B, Tonga GY, Ray M, Solfiell DJ and Rotello VM, MethodsX, 2015, 2, 306–315. [PubMed: 26151001]
24. Wu Y, Ali MRK, Chen K, Fang N and El-Sayed MA, Nano Today, 2019, 24, 120–140.
25. Ray M, Tang R, Jiang Z and Rotello VM, Bioconjug. Chem, 2015, 26, 1004–1007. [PubMed: 26011555]
26. Mout R, Ray M, Yesilbag Tonga G, Lee Y-W, Tay T, Sasaki K and Rotello VM, ACS Nano, 2017, 11, 2452–2458. [PubMed: 28129503]
27. Tang R, Wang M, Ray M, Jiang Y, Jiang Z, Xu Q and Rotello VM, J. Am. Chem. Soc, 2017, 139, 8547–8551. [PubMed: 28598151]
28. Roh YG, Shin SW, Kim S-Y, Kim S, Lim YT, Oh B-K and Um SH, Langmuir, 2019, 35, 3992–3998. [PubMed: 30844286]
29. Mout R, Ray M, Tay T, Sasaki K, Yesilbag Tonga G and Rotello VM, ACS Nano, 2017, 11, 6416–6421. [PubMed: 28614657]
30. Tang R, Jiang Z, Ray M, Hou S and Rotello VM, Nanoscale, 2016, 8, 18038–18041. [PubMed: 27738697]
31. Baimanov, Cai R and Chen C, Bioconjug. Chem, 2019, 30, 1923–1937. [PubMed: 31259537]
32. Givens BE, Wilson E and Fiegel J, Colloids Surf. B Biointerfaces, 2019, 179, 374–381. [PubMed: 30999116]
33. Rana S, Singla AK, Bajaj A, Elci SG, Miranda OR, Mout R, Yan B, Jirik FR and Rotello VM, ACS Nano, 2012, 6, 8233–8240. [PubMed: 22920837]
34. De M, Rana S, Akpinar H, Miranda OR, Arvizo RR, Bunz UHF and Rotello VM, Nat. Chem, 2009, 1, 461–465. [PubMed: 20161380]
35. Verma, Simard JM and Rotello VM, Langmuir, 2004, 20, 4178–4181. [PubMed: 15969414]
36. McCoy J, Chandana Epa V and Colman PM, J. Mol. Biol, 1997, 268, 570–584. [PubMed: 9159491]
37. Li Y, Zhang X and Cao D, Sci. Rep, 2013, 3, 3271. [PubMed: 24253561]
38. Rothemund PWK, Nature, 2006, 440, 297–302. [PubMed: 16541064]
39. Barnes E, Jenkins TA, Stein LM, Mathers RT, Wicaksana M, Pasquinelli MA and Savin DA, Biomacromolecules, 2020, 21, 2463–2472. [PubMed: 32378896]
40. Bai Y, Luo Q and Liu J, Chem. Soc. Rev, 2016, 45, 2756–2767. [PubMed: 27080059]
41. Piñeiro, Cordero OJ and Nogueira M, Peptides, 2000, 21, 1433–1446. [PubMed: 11072132]
42. Ma, Malessa A, Boersma AJ, Liu K and Herrmann A, Adv. Mater, 2020, 32, e1905309. [PubMed: 31943419]
43. McNaughton R, Cronican JJ, Thompson DB and Liu DR, Proc. Natl. Acad. Sci. U. S. A, 2009, 106, 6111–6116. [PubMed: 19307578]
44. Jahnke W and Erlanson DA, Eds., Fragment-based approaches in drug discovery, Wiley, 2006.
45. Tjandra KC and Thordarson P, Bioconjug. Chem, 2019, 30, 503–514. [PubMed: 30742420]

46. Santos PJ, Cao Z, Zhang J, Alexander-Katz A and Macfarlane RJ, J. Am. Chem. Soc, 2019, 141, 14624–14632. [PubMed: 31465688]
47. Simon J, Zhou Y, Ramasubramani V, Glaser J, Pothukuchy A, Gollihar J, Gerberich JC, Leggere JC, Morrow BR, Jung C, Glotzer SC, Taylor DW and Ellington AD, Nat. Chem, 2019, 11, 204–212. [PubMed: 30643229]
48. Mout R, Yesilbag Tonga G, Wang L-S, Ray M, Roy T and Rotello VM, ACS Nano, 2017, 11, 3456–3462. [PubMed: 28225593]
49. Bunz UHF and Rotello VM, Angew. Chem. Int. Ed Engl, 2010, 49, 3268–3279. [PubMed: 20405519]
50. You C-C, Miranda OR, Gider B, Ghosh PS, Kim I-B, Erdogan B, Krovi SA, Bunz UHF and Rotello VM, Nat. Nanotechnol, 2007, 2, 318–323. [PubMed: 18654291]
51. Jiang Z, Le NDB, Gupta A and Rotello VM, Chem. Soc. Rev, 2015, 44, 4264–4274. [PubMed: 25853985]
52. Phillips RL, Miranda OR, Mortenson DE, Subramani C, Rotello VM and Bunz UHF, Soft Matter, 2009, 5, 607–612.
53. Mereghetti P, Gabdoulline RR and Wade RC, Biophys. J, 2010, 99, 3782–3791. [PubMed: 21112303]
54. Brancolini, Polzi LZ, Corni S, J. Self-Assem. Mol. Electron. (SAME), 2015, 2, 1–26.
55. Huang R, Carney RP, Stellacci F and Lau BLT, Nanoscale, 2013, 5, 6928–6935. [PubMed: 23787874]
56. Park SJ, Int. J. Nanomedicine, 2020, 15, 5783–5802. [PubMed: 32821101]
57. Van Der Spoel, Lindahl E, Hess B, Groenhof G, Mark AE and Berendsen HJC, J. Comput. Chem, 2005, 26, 1701–1718. [PubMed: 16211538]
58. Gabdoulline RR and Wade RC, Biophys. J, 1997, 72, 1917–1929. [PubMed: 9129797]
59. Martinez M, Bruce NJ, Romanowska J, Kokh DB, Ozboyaci M, Yu X, Öztürk MA, Richter S and Wade RC, J. Comput. Chem, 2015, 36, 1631–1645. [PubMed: 26123630]
60. De M, Rana S and Rotello VM, Macromol. Biosci, 2009, 9, 174–178. [PubMed: 19127602]
61. Hong R, Emrick T and Rotello VM, J. Am. Chem. Soc, 2004, 126, 13572–13573. [PubMed: 15493887]
62. Brust M, Walker M, Bethell D, Schiffrin DJ and Whyman R, J. Chem. Soc. Chem. Commun, 1994, 0, 801–802.
63. Kanaras G, Kamounah FS, Schaumburg K, Kiely CJ and Brust M, Chem. Commun. (Camb.), 2002, 2294–2295. [PubMed: 12430408]
64. Templeton C, Wuelfing WP and Murray RW, Acc. Chem. Res, 2000, 33, 27–36. [PubMed: 10639073]
65. Kokh B, Corni S, Winn PJ, Hoefling M, Gottschalk KE and Wade RC, J. Chem. Theory Comput, 2010, 6, 1753–1768. [PubMed: 26615704]
66. Baker NA, Sept D, Joseph S, Holst MJ and McCammon JA, Proc. Natl. Acad. Sci. U. S. A, 2001, 98, 10037–10041. [PubMed: 11517324]
67. Gordon JC, Myers JB, Folta T, Shoja V, Heath LS and Onufriev A, Nucleic Acids Res, 2005, 33, W368–71. [PubMed: 15980491]
68. Elcock H, Gabdoulline RR, Wade RC and McCammon JA, J. Mol. Biol, 1999, 291, 149–162. [PubMed: 10438612]
69. Iori, Di Felice R, Molinari E and Corni S, J. Comput. Chem, 2009, 30, 1465–1476. [PubMed: 19037859]
70. Brancolini, Toroz D and Corni S, Nanoscale, 2014, 6, 7903–7911. [PubMed: 24882429]
71. Yang J, Yan R, Roy A, Xu D, Poisson J and Zhang Y, Nat. Methods, 2015, 12, 7–8. [PubMed: 25549265]

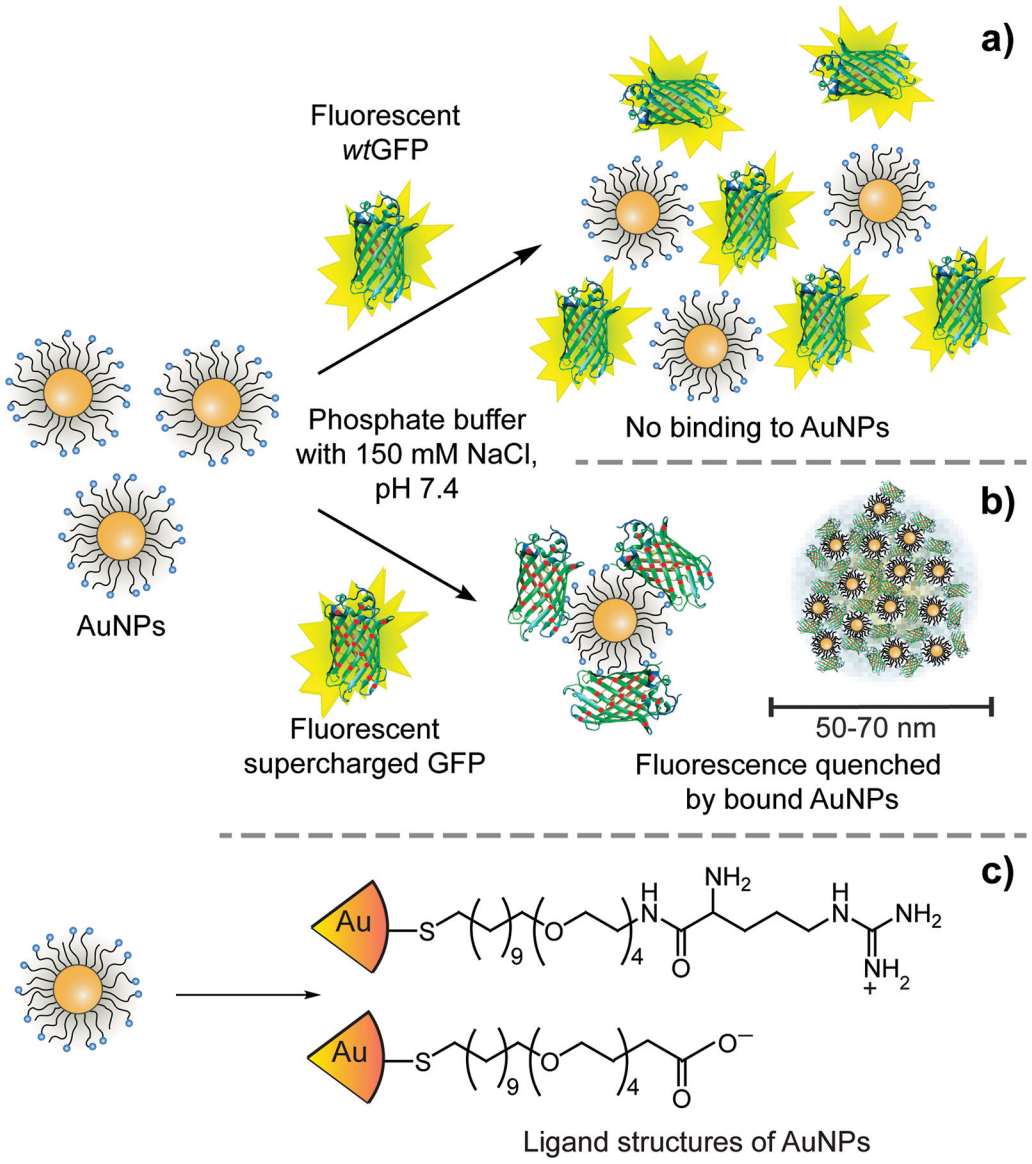

Fig. 1.

Schematic of the supramolecular interaction between AuNPs and supercharged GFPs. Fluorescence serves as an effective readout to quantify interaction between fluorescent proteins and nanoparticles. (a) *wt*GFP does not interact with AuNPs, and fluorescence remains ‘on’. (b) Supercharged GFP is bound by AuNPs, and fluorescence is quenched. (c) Charged nanoparticle ligands enable electrostatic interaction with other charged species.

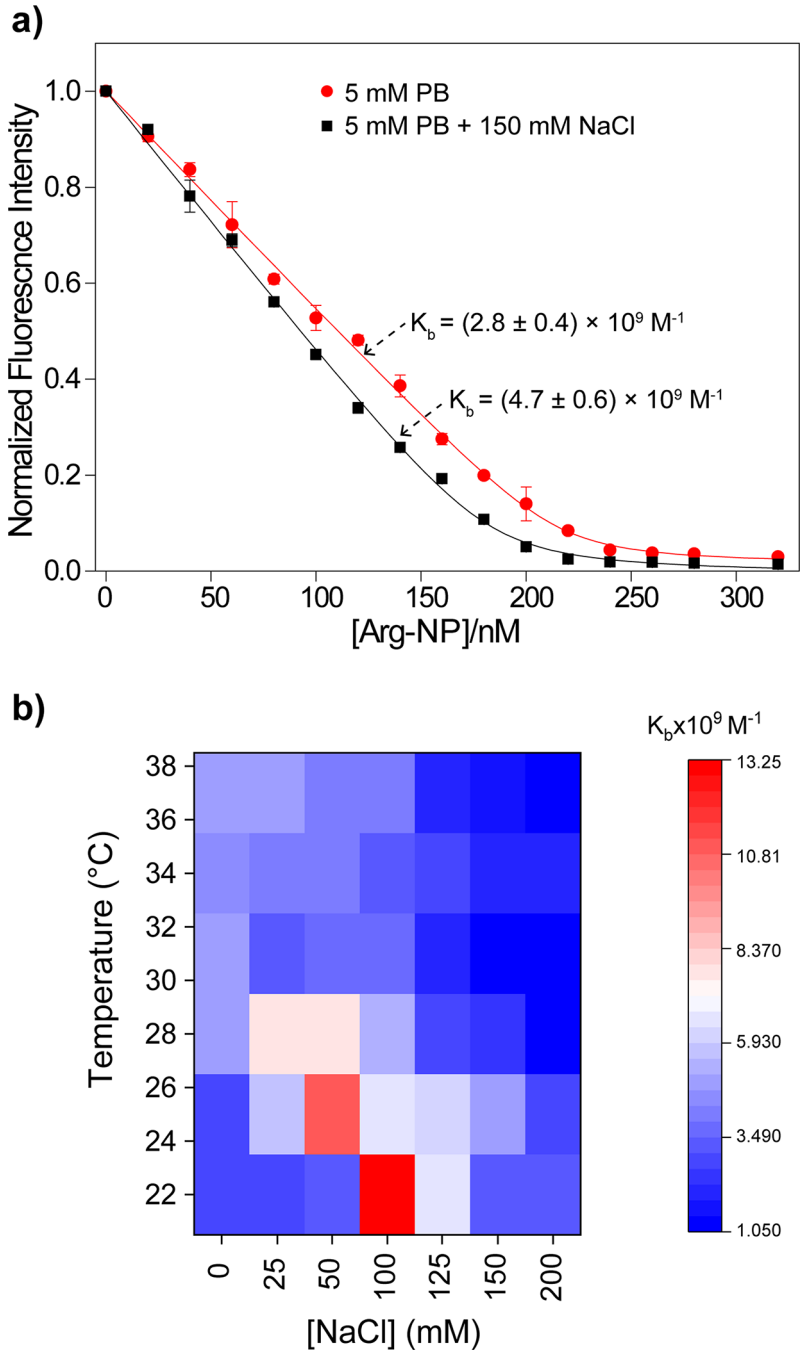

Fig. 2.

Interaction between Arg-NPs and −30GFP. (a) Fluorescence titrations between Arg-NPs and −30GFPs (50 nM) in 5 mM PB and in 5 mM PB containing 150 mM NaCl (pH 7.4) at 25°C. Complex binding constant (K_b) was determined using a previously reported method. (b) Responsiveness of the −30GFP: Arg-NPs interaction towards solution ionic strength at varied temperature; Fluorescence titrations between Arg-NPs and −30GFP (50 nM) were performed by parametrically varying temperature (22–37°C) and salt (NaCl, 0–200 mM) in 5 mM phosphate buffer. Error is shown as standard deviation by population.

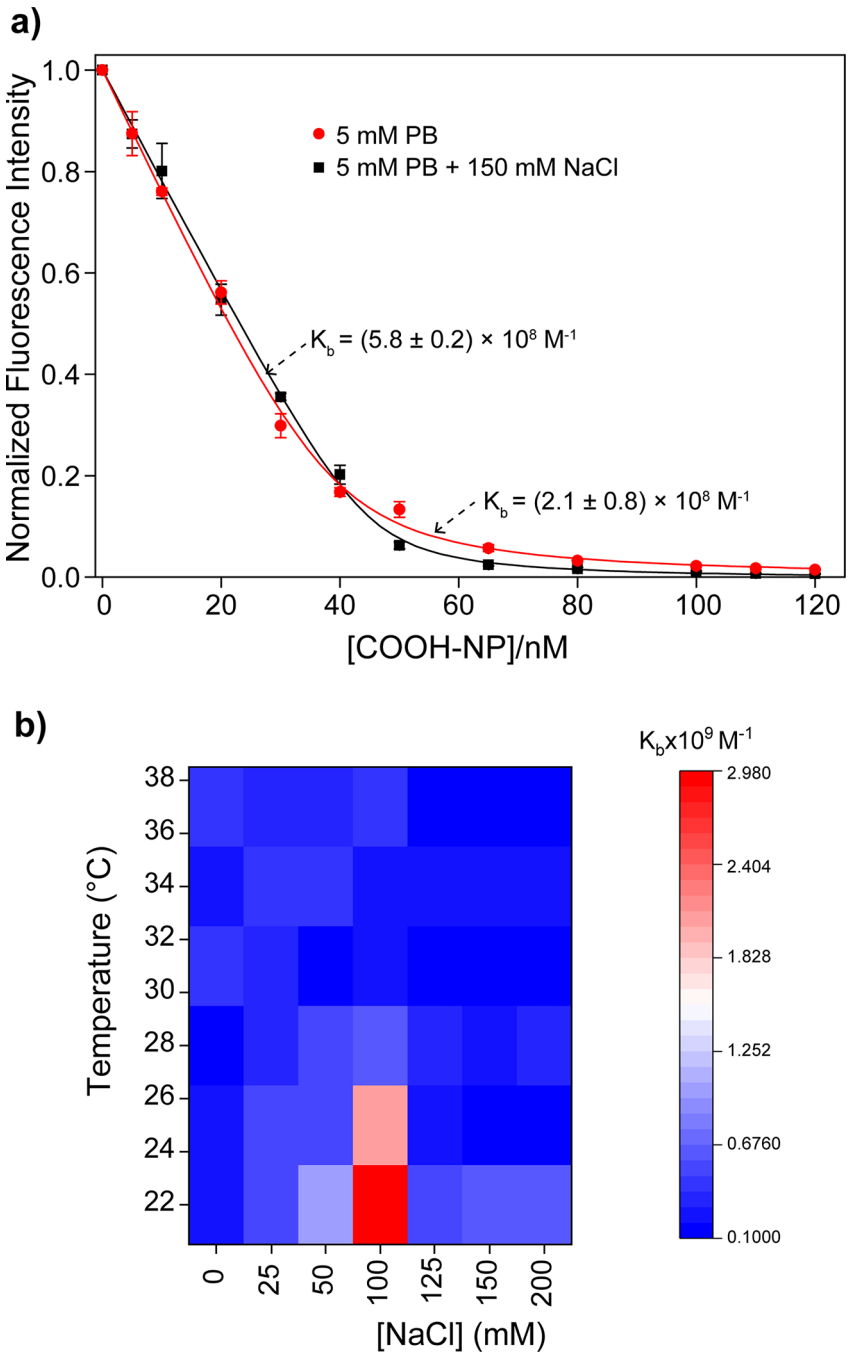

Fig. 3.

Interaction between COOH-NPs and +36GFP. (a) Fluorescence titrations between COOH-NPs and +36GFPs (50 nM) in 5 mM phosphate buffer and in 150 mM NaCl containing 5 mM phosphate buffer (pH 7.4) at 25°C. The complex binding constant (K_b) was determined using previously reported method. (b) Responsiveness of the +36GFP: COOH-NPs interaction towards solution ionic strength at varied temperature; Fluorescence titrations between Arg-NPs and +36GFP (50 nM) were performed parametrically varying temperature

(22–37°C) and salt (NaCl, 0–200 mM) in 5 mM PB. Error is presented as standard deviation by population.

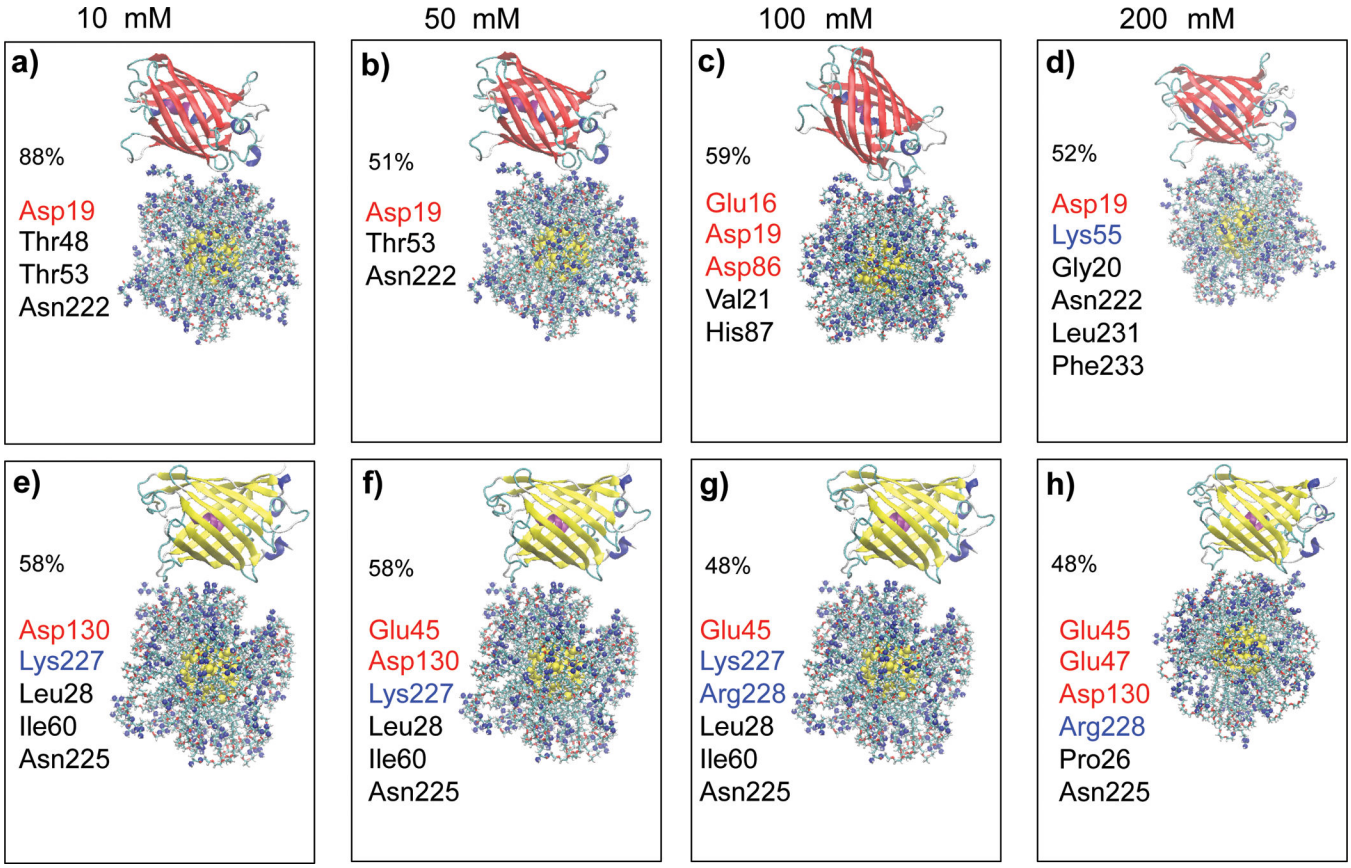

Fig. 4.

Top: Representative structure of the most populated complexes of −30GFP (structure in red) on cationic gold nanocluster $Au_{144}[L_{60}]^{+60}$ at different ionic strengths, obtained *via* BD simulation. Bottom: Representative structure of the most populated complexes of *wt*GFP (structure in yellow) on cationic gold nanocluster $Au_{144}[L_{60}]^{+60}$ at different ionic strengths. The relative population of the selected clusters is reported in percentage. Protein residues contacting the nanoparticle at short distances (less than 3.5 Å) are denoted with different colors based on charge, indicating neutral residues (black), positively charged residues (blue), and negatively charged residues (red). Protein backbone is shown in cartoon representation. AuNP and ligand are shown as van der Waals representations.

Table 1.

Summary of docking results of −30GFP: Arg-NP (a1–a4, b1–b4, c1–c5, and d1–d4), and *wt*GFP: Arg-NP interaction (e1–e4, f1–f4, g1–g3, and h1–h4) at varied ionic strength (IS); these represent the most populated complexes, which are ranked by size.

Label	RelPop *(a)* %	U_{Repr} *(b)*	U_{EP} *(c)*	U_{ds}^{e} *(d)*	U_{ds}^{h} *(e)*	spread *(f)*
−30GFP : Arg-NPs						
IS = 10 mM						
a1	88	−51.564	−39.788	3.205	−14.981	1.148
a2	10	−52.055	−40.060	3.841	−15.836	1.073
a3	1	−51.529	−37.736	3.901	−17.695	1.378
a4	1	−52.264	−35.432	3.158	−19.990	0.330
IS = 50 mM						
b1	51	−32.727	−20.431	2.811	−15.107	1.033
b2	41	−33.475	−19.764	3.071	−16.782	1.422
b3	6	−32.841	−17.140	2.602	−18.302	1.234
b4	2	−32.557	−20.107	3.324	−15.775	0.724
IS = 100 mM						
c1	59	−29.147	−15.138	3.134	−17.143	1.812
c2	33	−27.264	−13.685	2.662	−16.241	5.269
c3	5	−27.321	−15.409	2.808	−14.721	4.390
c4	3	−27.017	−14.768	3.334	−15.582	0.992
IS = 200 mM						
d1	52	−22.327	−9.227	2.936	−15.986	5.144
d2	35	−23.424	−10.045	3.410	−16.790	2.240
d3	8	−21.980	−8.826	2.962	−16.116	3.486
d4	4	−22.859	−11.282	4.277	−15.854	1.211
d5	1	−22.221	−10.508	3.977	−15.689	0.375
***wt*GFP : Arg-NPs**						
IS = 10 mM						
e1	58	−28.596	−16.088	3.297	−15.806	3.604
e2	30	−28.356	−15.471	3.608	−16.492	1.740
e3	8	−28.347	−16.486	3.992	−15.852	2.180
e4	2	−28.464	−15.924	4.448	−16.988	0.748
e5	2	−28.535	−16.422	3.173	−15.286	1.076
IS = 50 mM						
f1	58	−22.120	−9.839	2.899	−15.180	4.086
f2	37	−22.223	−9.544	3.544	−16.224	3.426
f3	5	−22.277	−9.656	4.138	−16.760	0.844
IS = 100 mM						
g1	48	−20.132	−7.108	2.695	−15.719	3.845
g2	46	−19.840	−6.825	3.089	−16.105	3.779

Label	RelPop [a] %	U_{Repr} [b]	U_{EP} [c]	U^{e}_{ds} [d]	U^{h}_{ds} [e]	spread [f]
g3	7	−19.473	−6.643	2.898	−15.727	2.155
IS = 200 mM						
h1	48	−18.242	−5.691	3.696	−16.247	3.701
h2	45	−16.233	−8.260	3.694	−11.667	7.161
h3	4	−16.462	−4.686	3.608	−15.384	7.861
h4	2	−16.816	−5.327	2.610	−14.099	2.174

[a] Relative population of the cluster

[b] U_{Repr}: total interaction energy of the representative of the given cluster, in kT with T= 300K

[c] U_{EP}: total electrostatic energy of the representative complex, in kT

[d] U^{e}_{ds}: electrostatic desolvation energy of the representative complex, in kT

[e] U^{h}_{ds}: non-polar (hydrophobic) desolvation energy of the representative complex, in kT

[f] RMSD of the structures within the cluster with respect to the representative complex.